2012

Self-assembly of single dielectric nanoparticle layers and integration in polymer-based solar cells

Jonathan E. Allen
Center for Functional Nanomaterials, Brookhaven National Laboratory, Upton, New York 11973, USA

Biswajit Ray
Purdue University - Main Campus, ray0@purdue.edu

Mohammad R. khan
Purdue University

Kevin G. Yager
Center for Functional Nanomaterials, Brookhaven National Laboratory, Upton, New York 11973, USA

Muhammad Ashraful Alam
Purdue University

See next page for additional authors

Allen, Jonathan E.; Ray, Biswajit; khan, Mohammad R.; Yager, Kevin G.; Alam, Muhammad Ashraful; and Black, Charles T., "Self-assembly of single dielectric nanoparticle layers and integration in polymer-based solar cells" (2012). *Birck and NCN Publications.* Paper 885.
http://dx.doi.org/10.1063/1.4744928

AIP | Applied Physics Letters

Self-assembly of single dielectric nanoparticle layers and integration in polymer-based solar cells

Jonathan E. Allen, Biswajit Ray, M. Ryyan Khan, Kevin G. Yager, Muhammad A. Alam et al.

Citation: Appl. Phys. Lett. **101**, 063105 (2012); doi: 10.1063/1.4744928
View online: http://dx.doi.org/10.1063/1.4744928
View Table of Contents: http://apl.aip.org/resource/1/APPLAB/v101/i6
Published by the American Institute of Physics.

Self-assembly of single dielectric nanoparticle layers and integration in polymer-based solar cells

Jonathan E. Allen,[1] Biswajit Ray,[2] M. Ryyan Khan,[2] Kevin G. Yager,[1] Muhammad A. Alam,[2] and Charles T. Black[1,a)]
[1]*Center for Functional Nanomaterials, Brookhaven National Laboratory, Upton, New York 11973, USA*
[2]*School of Electrical and Computer Engineering, Purdue University, West Lafayette, Indiana 47906, USA*

(Received 29 December 2011; accepted 26 July 2012; published online 6 August 2012)

A single, self-assembled layer of highly uniform dielectric alumina nanoparticles improves the photovoltaic performance of organic semiconductor bulk heterojunction solar cells. The block copolymer based self-assembly approach is readily amenable to the large areas required for solar cell fabrication. A fraction of the performance gain results from incident light scattering which increases active layer absorption and photocurrent output, consistent with device simulations. The nanoparticle layer also roughens the device electrode surface, increasing contact area and improving device fill factor through more efficient charge collection. © *2012 American Institute of Physics*. [http://dx.doi.org/10.1063/1.4744928]

A significant challenge associated with reducing solar cell active layer thicknesses from >100 microns in single-crystal silicon to ~100 nm in organic semiconductor materials is maintaining a maximum amount of incident light absorption.[1] Layers of nanoparticles can be used to scatter incident sunlight and improve absorption in thin-film solar cell active layers by increasing the optical path length within the active layer.[2–5] Metal nanoparticles have proven useful for this purpose, although engineering a net device performance benefit requires precise control of nanoparticle composition, shape, and dimensions to minimize losses due to resonant absorption by localized surface plasmons[2,6,7] and preventing them from degrading performance by acting as recombination centers. Dielectric nanoparticle layers also scatter light over a broad range of wavelengths in a manner favoring improved light absorption, without either the benefits or drawbacks associated with plasmonic properties.[2,7–10] Numerical studies suggest that dielectric scattering layers can outperform metal counterparts, especially for densely packed layers of high permittivity (ε_ρ), low absorption materials.[2]

In this work, we incorporate single layers of ~20 nm diameter close-packed dielectric alumina (Al_2O_3) nanoparticles ($\varepsilon_\rho \sim 10$) into an organic semiconductor bulk heterojunction device structure using a block copolymer self-assembly approach. Self assembly provides precise control over nanoparticle diameters and separations and is scalable to the large areas required for solar cell fabrication. Diblock copolymer thin films composed of polystyrene (PS) and poly(methyl methacrylate) (PMMA) (PS-*b*-PMMA) of suitable molecular weight ($M_n = 67$ kg/mol), mass ratio (70:30 PS:PMMA), and thickness (~25 nm) spontaneously self-organize into hexagonally-packed 20 nm diameter cylindrical PMMA domains (in a matrix of PS) with 40 nm nearest-neighbor spacing upon annealing at 200 °C for 3 h (in vacuum) (Figure 1(a)).[11,12] We promote perpendicular orientation of PMMA cylinders relative to the substrate by first treating the indium-tin oxide (ITO) substrate with a PS-*r*-PMMA random copolymer brush.[13]

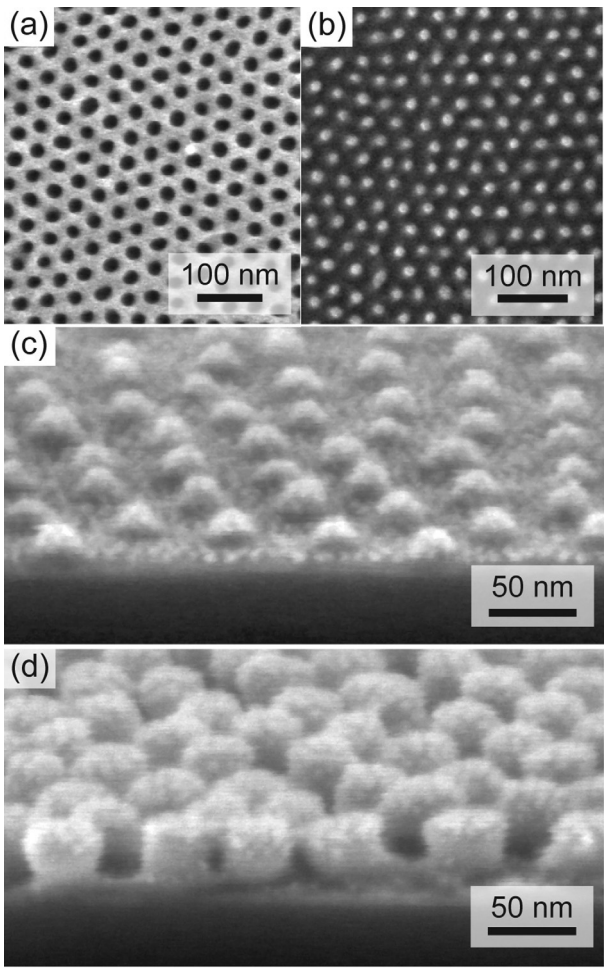

FIG. 1. (a) SEM image of a PS-b-PMMA block copolymer film. PMMA has been chemically removed to improve image contrast. (b) SEM image of alumina nanoparticle array fabricated by sequential exposure to three TMA/water cycles and removal of the organic material. (c), (d) 70 degree SEM images of alumina nanoparticle arrays: (c) 3 cycles and (d) 9 TMA/water cycles.

a)Author to whom correspondence should be addressed. Electronic mail: ctblack@bnl.gov.

We convert the 20 nm diameter PMMA domains into alumina nanoparticles by sequentially exposing the polymer-coated substrate to trimethylaluminum (TMA) (85 °C, 5 Torr, 1 min) and water vapor (85 °C, 5 Torr, 1 min). The TMA precursor selectively localizes within PMMA domains, leading to formation of a single layer of close-packed, uniformly sized alumina nanoparticles upon reaction with water (Figure 1(b)).[14,15] We repeat the sequence of precursor exposures to grow nanoparticles of progressively larger sizes. Nanoparticle cross sections start out roughly hemispherical for small numbers of exposure cycles (e.g., 3, in Figure 1(c)) and become more cylindrical with increasing numbers of cycles (e.g., 9, in Figure 1(d)). After formation of the alumina nanoparticle layer, we remove the remaining organic material using oxygen plasma (20 W rf power, 100 mTorr O_2). Analysis of scanning electron microscope (SEM) images reveals a 14 nm average nanoparticle diameter for 3 TMA/water precursor cycles, increasing and saturating at ~20 nm for larger numbers of cycles.

Organic semiconductor bulk heterojunction solar cells containing self-assembled alumina nanoparticle layers display improved power conversion efficiency compared to identical devices without nanoparticles. Our device structure consists of an ITO-coated glass substrate (160 nm ITO) having a 20 nm thick TiO_2 (anatase) electron contact layer, grown by atomic layer deposition. The alumina nanoparticle layer is positioned on the ITO surface and is conformally coated by the TiO_2 electron contact. We spin-cast ~100 nm thick blend active layers of poly(3-hexylthiophene) and [6,6]-phenyl-C_{61}-butyric acid methyl ester (P3HT:PCBM, 1:1 wt.) from chlorobenzene prior to forming a top contact of spin-cast poly(3,4-ethylenedioxythiophene)poly(styrenesulfonate) (PEDOT:PSS) (40 nm) and thermally evaporated Au (80 nm). SEM cross-sectional images show that the nanoparticles introduce a significant degree of controlled roughness into the TiO_2 electron collecting contact (Figures 2(a) and (b)). Representative current-voltage measurements (*J-V*) of devices with and without nanoparticle layers (3 TMA/water cycles, in this case) in the dark and under simulated solar illumination show that introducing the nanoparticles improves the photovoltaic power conversion efficiency (Figure 2(c)) (illumination in ambient conditions by 70 mW/cm^2 simulated AM1.5 G sunlight, calibrated using a certified KG5 filtered silicon reference cell). On average, devices showed a 10% increase in photocurrent density over an identical device without nanoparticles (from 5.1 to 5.6 ± 0.2 mA/cm^2) and a 25% improvement in power conversion efficiency (from 2.3 to 2.9 ± 0.1%), based on measurements of 3-5 devices of each type. The efficiency of our devices is lower than the best reported values for inverted P3HT:PCBM solar cells, primarily because of reduced photocurrent due to an unoptimized P3HT:PCBM layer thickness. Other metrics such as open circuit voltage and fill factor are comparable with those of higher performing devices.

Optical spectroscopy measurements show that P3HT:PCBM layers deposited on roughened TiO_2 layers with underlying nanoparticles transmit less light compared to films on smooth TiO_2 (Figure 2(d)), consistent with scattering by the dielectric particles. The integrated light transmission (from 350 nm to 900 nm) through the sample

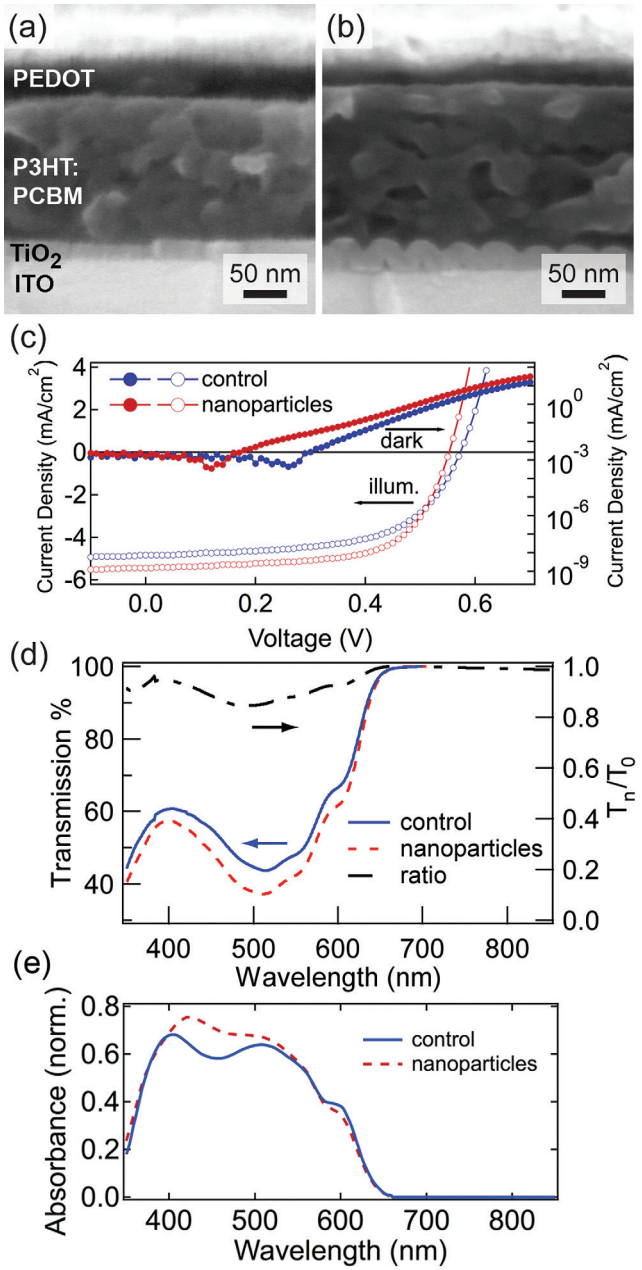

FIG. 2. (a), (b) Cross sectional images of P3HT:PCBM devices (a) without, and (b) with nanoparticle layers. (c) Representative dark (solid) and illuminated (open) *J-V* characteristics of solar cells without (blue) and with (red) a nanoparticle layer. (d) Optical transmission through P3HT:PCBM blend films formed on substrates without (blue, solid) and with (red, dashed) a nanoparticle layer. Dashed black curve is the ratio of the two spectra. (e) Simulated optical absorbance spectra of P3HT:PCBM active layers on substrates without (blue, solid) and with (red, dashed) a nanoparticle layer.

containing alumina particles is 13% smaller than that of a P3HT:PCBM film deposited on smooth TiO_2, meaning that 13% fewer photons transmit directly through the sample. Two-dimensional, full-wave optical simulations of the device structure (COMSOL-RF module) show that the dielectric nanoparticle layer results in an additional 5%-6% integrated light absorption by the P3HT:PCBM active layer (Figure 2(e)), in qualitative agreement with the measured 10% photocurrent increase (Figure 2(b)). The decrease in light transmission in samples containing nanoparticles is relatively constant across the wavelength spectrum (Figure 2(d)),

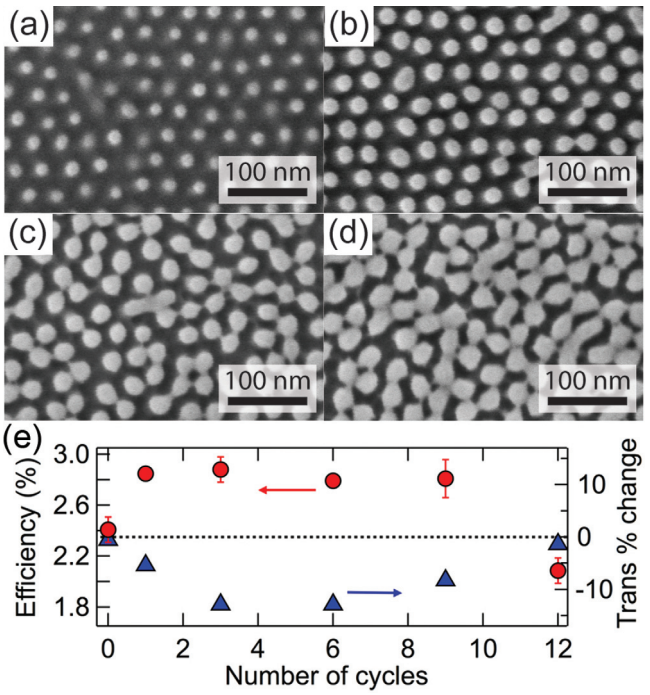

FIG. 3. (a)-(d) SEM images of alumina nanoparticle layers formed using (a) 3, (b) 6, (c) 9, and (d) 12 TMA/water cycles. (e) Photovoltaic power conversion efficiency (red circles) and percentage change in integrated optical transmission (blue triangles) versus number of TMA/water cycles. Data points are an average of 3-5 devices with error bars indicating standard deviation.

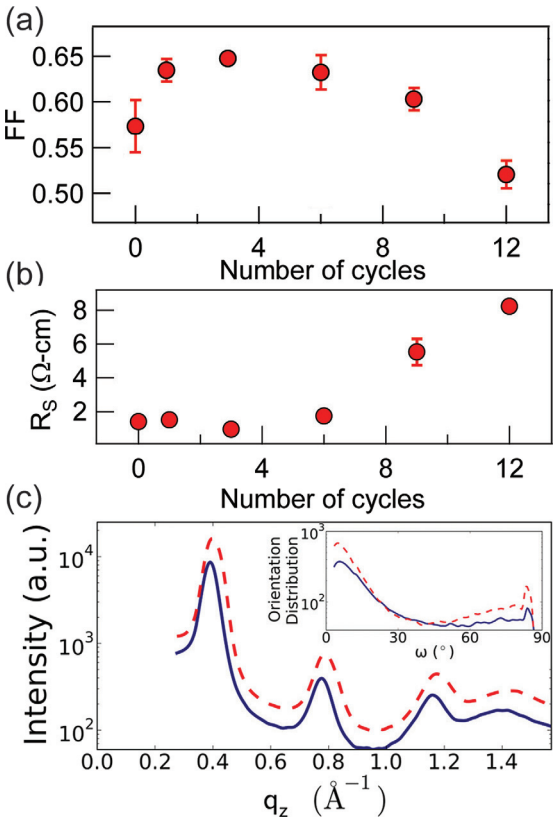

FIG. 4. (a) Device fill factor versus number of TMA/water cycles. (b) Device total resistance (unilluminated) versus number of TMA/water cycles. Data points are an average of 3 to 5 devices with error bars indicating standard deviation. (c) GIXRD data comparing P3HT:PCBM blend films on smooth TiO_2 films (blue, solid) versus TiO_2 roughened by underlying nanoparticle layer (red, dashed). Inset: Orientation distribution for (100) scattering peak, as function of meridional angle ω (where $\omega = 0°$ is film normal (q_z) direction).

consistent with previous reports showing that scattering from slightly larger dielectric nanoparticles (SiO_2) is spectrally uniform.[7]

Varying the number of TMA/water exposure cycles used to form the nanoparticle layer from one to nine (Figures 3(a)–3(d)) does not significantly change the device photovoltaic performance. A single TMA/water exposure cycle forms an array of nanoparticles having ill-defined diameters (fuzzy boundaries in images of Figure 3(a)), yet still increases the average power conversion efficiency by 19% over a device without particles. Increasing numbers of TMA/water exposure cycles better define nanoparticle boundaries while also increasing both the diameter and height (Figures 3(b)–3(d)). Beyond ~9 TMA/water cycles, the resulting array is distorted from the initial self-assembled polymer pattern with some particles fusing together, likely due to stress induced by high precursor loading within the initial PMMA domain (Figures 3(c) and 3(d)). P3HT:PCBM devices having nanoparticle arrays formed using between one and nine TMA/water exposure cycles all show, on average, an 20%–25% higher power conversion efficiency compared to an identical devices without nanoparticles (Figure 3(e)). Devices with a layer of nanoparticles formed using 12 TMA/water cycles have decreased performance (Figure 3(e)) due to a large series resistance that results from significant numbers of alumina islands fusing together to create an insulating film between electrode and active layer. Ultraviolet-visible spectroscopy shows decreased light transmission through P3HT:PCBM films deposited on TiO_2 layers with underlying particle arrays created by 1, 3, 6, and 9 TMA/water cycles (Figure 3(e)), but essentially no change in transmission through films on particle arrays made from 12 TMA/water cycles.

The 10%–13% photocurrent increase accounts for half of the 25% improvement in P3HT:PCBM solar cell efficiency, indicating benefits of the nanoparticle layer beyond increased light scattering. Despite containing electrically insulating nanoparticle arrays between the ITO and TiO_2 electron contact layer, devices with nanoparticles have significantly improved fill factor (FF) (Figure 4(a)). For example, devices containing particle arrays made using 3 TMA/water cycles show an average FF increase of 14%, from 0.57 to 0.65. Simulations of charge carrier transport in our devices, calculated by using self-consistent numerical solution of drift-diffusion and Poisson equations,[16] show that the improved FF is a natural consequence of reduced electron collection distance, due to the TiO_2 layer projecting slightly into the P3HT:PCBM blend. Our charge recombination model includes both band-to-band recombination (bimolecular recombination coefficient $= 10^{-10}$ cm^3) and trap-assisted recombination ($\tau_{SRH} = 1\,\mu$s). Although simulations show that changes in the device geometry naturally account for the observed FF improvement, we cannot definitively rule out the role of other structural factors such as changes in the P3HT:PCBM blend distribution.

Under high forward voltage bias (>1.5 V), the total device resistance (R_S) is little changed by addition of

nanoparticle arrays made using fewer than 9 TMA/water cycles (Figure 4(b)). Because the device resistance at high dark current is dominated by the contacts, the relative invariance of R_S means that for sufficiently small numbers of cycles ($\sim$6), the contact resistances are not negatively impacted by the introduction of nanoparticles. Particle arrays made from greater numbers of TMA/water cycles introduce a sharp increase in forward bias resistance as shrinking inter-particle separations limit the interfacial area between TiO_2 and ITO layers. From geometric considerations of the hexagonal nanoparticle arrangement, we find the TiO_2 layer resistance scales as $R_S \propto L/[1-(\pi/2\sqrt{3})(d/\ell)^2] \approx L/[1-0.9(d/\ell)^2]$ with ℓ the center-to-center interparticle separation and L the TiO_2 layer thickness, which grows with nanoparticle height. Increased R_s with large number of TMA/water exposure cycles creates a sharp drop in device FF (Figure 4(a)), resulting in a steep decline in device power conversion efficiency (Figure 3(e)).

Structural analysis by grazing incidence x-ray diffraction shows that the crystalline P3HT structure on roughened TiO_2 substrates changes only slightly from that on a smooth surface (Figure 4(c)). The average P3HT grain size (17 nm), determined from the width of the (100) scattering peak,[17] is nearly unchanged. We can exclude any P3HT chain reorientation, which would significantly change the out-of-plane electronic mobility,[18] because the molecular orientation distribution is unaffected by substrate roughness (inset of Figure 4(c)).

Introducing the nanoparticle layer into the structure reduces the device open circuit voltage (V_{oc}) by 4% (from 0.57 V to 0.55 V). The lower V_{oc} reflects the increased device dark current (Figure 2(c)), which is $\sim$1 mA/cm^2 higher in the nanoparticle containing device at V_{oc}, compared to the control device. Although the increased dark current could in principle be attributed to increased recombination at the rough nanoparticle interface, our extensive numerical simulation shows that such recombination, by itself, is inconsistent with the simultaneous systematic improvement in J_{sc} and FF. The only self-consistent hypothesis that explains the complete J-V characteristics is a slight ($\sim$1%) reduction in the P3HT optical bandgap ($\sim$25 meV) once the nanoparticles are introduced into the device. Small changes in P3HT packing structure could conceivably translate into changes in bandgap. For example, density functional theory calculations have shown that torsional defects within P3HT chains can shift the bandgap by energies of this order.[19] The lower bandgap allows injection of additional carriers, accounting for the increased dark current (and thus reduced V_{oc}) and also providing additional light absorption (and photocurrent output). Combined with improved absorption due to light scattering (Fig. 1(e)) and enhanced FF (associated with better charge collection by slightly projected electrodes), the numerical simulation explains the efficiency gain as well as all aspects of the J-V data self-consistently. Additional high precision characterization of bandgap therefore will be an important part of future study regarding this subject.

Research carried out in part at the Center for Functional Nanomaterials, Brookhaven National Laboratory, which is supported by the U.S. Department of Energy, Office of Basic Energy Sciences, under Contract No. DE-AC02-98CH10886. The authors (B.R., M.R.K, and M.A.A) gratefully acknowledge financial support from the DOE-ERFC at Columbia University (No. DE SC0001085).

[1]H. R. Stuart and D. G. Hall, J. Opt. Soc. Am. A **14**(11), 3001–3008 (1997).
[2]Y. A. Akimov, W. S. Koh, S. Y. Sian, and S. Ren, Appl. Phys. Lett. **96**(7), 073111 (2010).
[3]H. A. Atwater and A. Polman, Nat. Mater. **9**(3), 205–213 (2010).
[4]K. R. Catchpole and A. Polman, Appl. Phys. Lett. **93**(19), 191113 (2008).
[5]P. Matheu, S. H. Lim, D. Derkacs, C. McPheeters, and E. T. Yu, Appl. Phys. Lett. **93**(11), 113108 (2008).
[6]K. Nakayama, Appl. Phys. Lett. **93**(12), 121904 (2008).
[7]S. P. Sundararaian, N. K. Grady, N. Mirin, and N. J. Halas, Nano Lett. **8**(2), 624–630 (2008).
[8]T.-H. Chang, P.-H. Wu, S.-H. Chen, C.-H. Chan, C.-C. Lee, C. C. Chen, and Y.-K. Su, Opt. Express **17**(8), 6519–6524 (2009).
[9]J. R. Nagel and M. A. Scarpulla, Opt. Express **18**(13), A139–A146 (2010).
[10]C.-P. Chen, P.-H. Lin, L.-Y. Chen, M.-Y. Ke, Y.-W. Cheng, and J. J. Huang, Nanotechnology **20**(24), 245204 (2009).
[11]K. W. Guarini, C. T. Black, and S. H. I. Yeuing, Adv. Mater. **14**(18), 1290 (2002).
[12]T. Thurn-Albrecht, R. Steiner, J. DeRouchey, C. Stafford, E. Huang, M. Bal, M. Tuominen, C. Hawker, and T. Russell, Adv. Mater. **12**(11), 787–791 (2000).
[13]P. Mansky, Y. Liu, E. Huang, T. Russell, and C. Hawker, Science **275**(5305), 1458–1460 (1997).
[14]Q. Peng, Y.-C. Tseng, S. B. Darling, and J. W. Elam, Adv. Mater. **22**(45), 5129 (2010).
[15]Q. Peng, Y.-C. Tseng, S. B. Darling, and J. W. Elam, ACS Nano **5**(6), 4600–4606 (2011).
[16]B. Ray and M. A. Alam, Sol. Energy Mater. Sol. Cells **99**, 204–212 (2012).
[17]D.-M. Smilgies, J. Appl. Crystall. **42**, 1030 (2009).
[18]J. E. Allen, K. G. Yager, H. Hlaing, C. Y. Nam, B. M. Ocko, and C. T. Black, Appl. Phys. Lett. **99**, 163301 (2011).
[19]S. B. Darling, J. Phys. Chem. B **112**(30), 8891–8895 (2008).